European Journal of Pharmaceutics and Biopharmaceutics 216 (2025) 114873

Contents lists available at ScienceDirect

European Journal of Pharmaceutics and Biopharmaceutics

journal homepage: www.elsevier.com/locate/ejpb

Research paper

Structural insights into novel coamorphous systems of azithromycin with faster dissolution profile

Ilenia D'Abbrunzo [a], Ludovica Battaiotto [a], Angela Abruzzo [b], Giulia Bondi [b], Federica Bigucci [b], Cinzia Pagano [c], Anna Imbriano [c], Costanza Fratini [d], Luca Casettari [d], Dario Voinovich [a], Dritan Hasa [a,*]

[a] Department of Chemical and Pharmaceutical Sciences, University of Trieste, P.le Europa 1, Trieste 34127, Italy
[b] Department of Pharmacy and Biotechnology, University of Bologna, Via S. Donato 19/2, Bologna 40127, Italy
[c] Department of Pharmaceutical Sciences, University of Perugia, via del liceo 1, Perugia 06123, Italy
[d] Department of Biomolecular Sciences, School of Pharmacy, University of Urbino Carlo Bo, Via Ca le Suore 2 - 61029 Urbino (PU), Italy

ARTICLE INFO

Keywords:
Azithromycin
Coamorphous
Multicomponent solids
Pair distribution function
In vitro dissolution tests

ABSTRACT

In this study, azithromycin, a broad-spectrum antibiotic compound used for the treatment of several bacterial infections, which is characterized by a very low water solubility, was combined with different small molecules to generate more soluble coamorphous solids. The multicomponent systems were prepared through fast precipitation from an ethyl acetate solution, facilitating the formation of amorphous phases in seven azithromycin-based systems. Differential scanning calorimetry confirmed the coamorphous nature in five out of seven systems (i.e., azithromycin–2-, 3-, and 4-aminobenzoic acids, –salicylic acid, –caprylic acid), while two systems (azithromycin–methyl salicylate, –glycerol) exhibited ambiguous thermal behavior. Stability assessments revealed that the homogeneous coamorphous systems remained stable for at least 140 days at 40 °C, while pure amorphous azithromycin, recrystallized within 72 h. The most suitable coamorphous systems were characterized through pair distribution function analysis, providing molecular-level insights into their structural organization. Notably, the azithromycin–caprylic acid system exhibited distinct molecular packing, likely attributable to the unique structural characteristics of its fatty acid-based coformer, which also led to a faster drug dissolution rate compared to the pure crystalline and amorphous azithromycin forms.

1. Introduction

Macrolides are a well-known class of antibiotics characterized by a broad-spectrum efficacy and relatively low toxicity [1]. Among these, azithromycin (AZT) (Fig. 1) is widely used to treat various bacterial infections, a prolonged half-life (68 h) that permits a once-daily dosing, and a lower incidence of side effects and drug interactions [2].

AZT is available in several formulations including capsules, tablets, and oral suspensions. While the bioavailability of capsules is affected by gastric filling, tablets and suspensions maintain consistent bioavailability regardless of food intake [2]. As a broad-spectrum antibiotic, AZT is effective against both gram-positive and gram-negative bacteria and is particularly used in pediatric care for several infections such as respiratory tract infections, pharyngitis, and otitis due to its favorable safety profile. However, AZT mainly presents three problems that limit its therapeutic efficacy as well as patient compliance: i) the unfavorable dissolution profile responsible for the limited bioavailability [4]; ii) limited gastrointestinal permeability, which hinders absorption and impacts therapeutic outcomes [5]; iii) bitter taste representing a substantial barrier in pediatric applications, often leading to reduced adherence to prescribed regimens [6].

To address these limitations, various approaches have been explored,

Abbreviations: AZT, azithromycin; CSD, Cambridge Structural Database; ERT, erythritol; GLY, glycerol; GLU, glucose; FRU, fructose; ASP, aspartame; NEO, neotame; A2AB, 2- aminobenzoic acid; A3AB, 3- aminobenzoic acid; A4AB, 4-aminobenzoic; ASLC, salicylic acid; MSLC, methyl salicylate; D-MAL, D-malic acid; L-MAL, L-malic acid; ACP, capric acid; ACPL, caprylic acid; PXRD, powder X-ray diffraction; DSC, differential scanning calorimetry; PDF, pair distribution function analysis; EA, ethyl acetate; ACN, acetonitrile; PVDF, polyvinylidene fluoride reducer; T_g, glass transition temperature; R.T., room temperature; ESRF, European Synchrotron Radiation Facility, HPLC, high-performance liquid chromatography.

* Corresponding author at: Department of Chemical and Pharmaceutical Sciences, University of Trieste, P.le Europa 1, Trieste 34127, Italy.
E-mail address: dhasa@units.it (D. Hasa).

https://doi.org/10.1016/j.ejpb.2025.114873
Received 24 April 2025; Received in revised form 3 July 2025; Accepted 19 September 2025
Available online 21 September 2025

including the use of cocrystallization technology with other active ingredients [7,8], taste-masking agents to reduce bitterness [9], salt formation to enhance aqueous stability [10,11], solid dispersions with polymeric carriers to increase the dissolution and to limit the bitterness [12–15], inclusion complexes with cyclodextrin to boost solubility and stability [16,17], and nanoparticulate/lipid-based formulations to obtain a controlled release and to improve the bioavailability [18–21].

Moreover, two amorphous forms of AZT have been reported in literature, which can be obtained either through melt quenching or by dehydration of the thermodynamically stable and commercially available dihydrate (indexed in the Cambridge Structural Database (CSD) with refcode GEGJAD02 [22]).

Despite the extensive development of multicomponent systems and the identification of amorphous forms of pure AZT, the use of coamorphization strategy, i.e., the production of homogeneous amorphous multicomponent materials [23–30], has not been reported to date.

Coamorphous systems represent an effective strategy for overcoming the solubility limitations of crystalline drugs [23–30]. By combining a specific drug with suitably selected coformers, it is possible to enhance the physical stability of the amorphous phase through non-covalent interactions, and at the same time, improve the dissolution kinetics of the drug compared to its pure crystalline form [23–28,31–41]. This dual advantage of improved solubility and stability opens new avenues for the design of advanced multicomponent amorphous materials, tailored to address critical pharmaceutical challenges.

Building on these considerations, and given the existence of coamorphous systems of antibiotics with improved properties [42–45], this study probed the possibility of developing coamorphous systems of AZT. The selection of the coformers was primarily guided by the three main limitations of AZT discussed above, and a library of 14 possible coformers was used during the screening stage (Fig. 2).

Among the tested combinations, seven coamorphous systems of AZT were successfully obtained and initially characterized using standard solid-state techniques, namely powder X-ray diffraction (PXRD), differential scanning calorimetry (DSC) and physical stability tests. Systems that resulted in crystalline phases or showed poor physical stability were not considered for further investigation. Subsequently, the multicomponent products showing suitable solid-state properties, were characterized using pair distribution function (PDF) analysis to elucidate the atomic and molecular interactions across short, medium, and long-range distances. Finally, *in vitro* dissolution tests were conducted to evaluate the dissolution ability of the selected coamorphous systems with respect to the API in its crystalline or amorphous forms.

2. Materials and methods

2.1. Materials

AZT, (2R,3S,4R,5R,8R,10R,11R,12S,13S,14R)-11-[(2S,3R,4S,6R)-4-(dimethylamino)-3-hydroxy-6-methyloxan-2-yl]oxy-2-ethyl-3,4,10-trihydroxy-13-[(2R,4R,5S,6S)-5-hydroxy-4-methoxy-4,6-dimethyloxan-2-yl]oxy-3,5,6,8,10,12,14-heptamethyl-1-oxa-6-azacyclopentadecan-15-one, and the molecules used as coformers (Fig. 2) were obtained from Sigma-Aldrich (St. Louis, USA). Ethyl acetate (EA) was purchased from Carlo Erba (Rodano, Milan, Italy), while acetonitrile (ACN) was bought from Sigma-Aldrich (St. Louis, USA). All the actives and chemicals were used without further purification.

2.2. Methods

2.2.1. Samples preparation

2.2.1.1. Mechanochemical experiments. Mechanochemical experiments were performed in Retsch MM200 vibrational mill (Retsch, Germany) equipped by two 14 mL stainless steel jars and two 7 mm Ø beads, respectively. The milling frequency for each pathway was maintained at 25 Hz, the void volume in the jar was also kept constant (i.e., a total of 250 mg of powder per jar) and the milling time was kept fixed (i.e., 60 min). AZT was milled with each coformer in a 1:1 M ratio in the presence of 60 μL (η [46] = 0.24) of two liquids with different polarity namely EA and ACN.

2.2.1.2. Solution-based methods. About 50 mg of powder (pre-milled for cosystems or commercial-grade powder for pure AZT) was dissolved in 15 mL of EA. The solvent was subsequently removed using rotary evaporation to facilitate precipitation, thus the formation of amorphous systems. The employed instrument was a Buchi R-210 rotary evaporator equipped with a Laboxact vacuum pump. Each evaporation process lasted approximately 30 min.

2.2.2. Samples characterization

2.2.2.1. PXRD analysis. PXRD analyses were performed using a Bruker D2 Phaser benchtop diffractometer (Bruker, Manheim, Germany) operating in Bragg-Brentano geometry with Cu-Kα radiation (λ = 1.5418 Å) from a 300 W low-power X-ray source (30 kV, 10 mA). Data were collected over a 2θ range of 5-35°, with a step size of 0.02° and a scan speed of 0.6°/s. Each sample was prepared by carefully pressing around 200 mg of the ground product into a steel sample holder fitted with a cylindrical polyvinylidene fluoride (PVDF) reducer. In cases where the

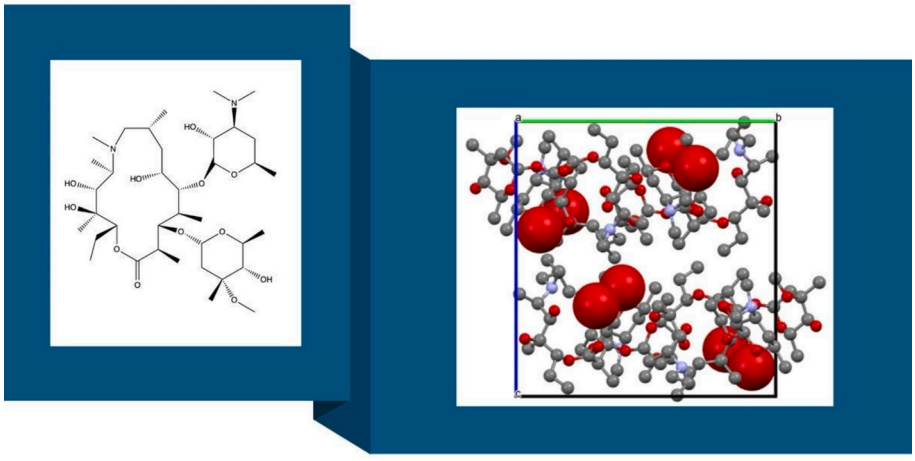

Fig. 1. Azithromycin molecular structure (left) and crystalline packing (right) [3].

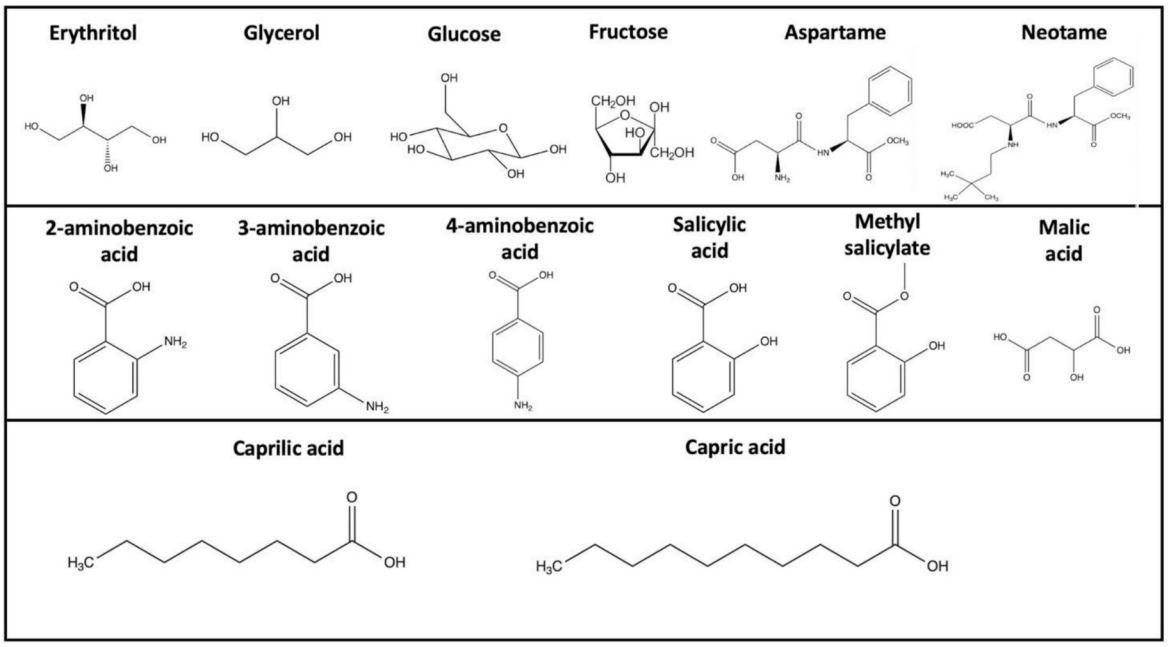

Fig. 2. Molecular structures of the coformers selected in this study.

recovery of milled samples was limited and for stability tests, a "zero background" sample holder coated with silicone resin was used.

2.2.2.2. DSC analysis. For DSC analyses, samples weighing 2–4 mg were placed in 40 μL aluminum crucibles that were sealed and pierced. The analyses were performed using a Mettler Toledo DSC 3 Star^e System (Milan, Italy). Standard characterization involved heating ramps starting at 25 °C and progressing to approximately 20 °C above the expected melting point of the sample, with the exact endpoint depending on the coformer used. The heating rate was set at 10 °C/min under a constant N_2 flow of 50 mL/min. To determine the glass transition temperature (T_g), heating–cooling–heating cycles were performed. The first heating phase followed the same parameters as the standard characterization, ensuring the complete melting of the sample. This was followed by a 5-min isothermal hold to stabilize the molten state. Rapid cooling at a rate of 50 °C/min was then applied to produce an amorphous material. Finally, a second heating ramp, identical to the first, was performed to identify the T_g, which was expressed as inflection point in the thermal curve.

2.2.2.3. Physical stability tests under stressed conditions. The physical stability of the coamorphous systems [23,41,47] was monitored over a 140-day period at room temperature (R.T.). Additional stability tests were carried out under accelerated conditions (40 °C) to evaluate their behavior under more severe thermal stress. Samples were collected weekly during the first month and biweekly thereafter, with each sample analyzed for potential recrystallization using PXRD, as reported in section 2.2.2.1.

2.2.2.4. PDF analysis. The high-resolution X-ray diffraction and scattering measurements were performed at the European Synchrotron Radiation Facility (ESRF) [48]. Powder samples were placed in cylindrical slots (approximately 1 mm thick) between Kapton windows and mounted in a high-capacity sample holder. Each sample was measured in transmission geometry using X-rays at an energy of 75.051 keV (λ = 0.16520 Å). Intensity data were recorded using a Pilatus CdTe 2 M detector (1679 × 1475 pixels, 172 × 172 μm^2 each), positioned with the incident beam aligned to the detector corner. The sample-to-detector distance was set to 1.5 m for high-resolution measurements and 0.3 m for total scattering measurements. Background noise from empty windows was measured and subtracted.

For geometric calibration, NIST SRM 660b (LaB_6) was used, and image integration was carried out with pyFAI software [49], which included corrections for flat-field, geometry, solid angles, and polarization.

2.2.2.5. In vitro dissolution tests. *In vitro* dissolution tests were conducted by placing an appropriately weighed amount (equivalent to 15mg of pure AZT) of the coamorphous systems or pure AZT (crystalline or amorphous) in 15 mL of phosphate buffer (KH_2PO_4 0.2 M adjusted at pH 6.8 with KOH 300 g/L) in a closed glass vial, thermostated at 37 °C ± 0.5 °C. The mixture was stirred at 250 rpm and at fixed intervals of time (2, 5, 10, 15, 30, 60, 120, 180, 240, 300 and 360 min) aliquots (0.2 mL) were withdrawn and immediately replaced with an equal volume of fresh medium. The samples were adequately diluted with methanol and analyzed through high-performance liquid chromatography *(HPLC)*. The experiments were performed in triplicate and results are shown as percentage of dissolved drug plotted as a function of time. For dissolution results, *t*-test was used to determine statistical significance. The criterion for statistical significance was $p < 0.05$.

2.2.2.6. HPLC analysis. AZT quantification through HPLC was performed following the method previously reported [50]. Briefly, the chromatographic system was based on a Shimadzu (Milan, Italy) LC-10ATVP chromatographic pump and a Shimadzu SPD-10AVP UV–vis detector set at 215 nm. A Phenomenex (Torrance, CA, USA) Kinetex (150 mm × 4.6 mm I.D., 5 mm) was used as column and coupled to a Phenomenex (Torrance, CA, USA) Security Guard C18 guard cartridge (4 mm × 3.0 mm I.D., 5 mm). The mobile phase was composed of phosphate buffer (KH_2PO_4 0.01 M adjusted at the pH 7.5 with 10 M KOH), methanol and acetonitrile (10/50/40, v/v). The flow rate of the mobile phase was set at 0.8 mL/min and the injected volume was 20 μL. In these conditions, the retention time of AZT was 4.7 min.

3. Results and discussion

The choice of suitable experimental conditions for obtaining coamorphous multicomponent solids of AZT was guided by the study of Kui

Chen and collaborators [51]. In that study, the authors observed that AZT exhibits distinct morphological outcomes based on the solvent used. Specifically, AZT undergoes a spheronization process in water, forming solid spheres with dense internal structures, while hollow spheres are obtained when AZT is precipitated from EA. Such intriguing behavior was attributed to the differential solvent evaporation dynamics and solute–solvent interactions in the two media. The authors used the term "*bridging liquid*", to describe the role of EA on mediating interactions between molecules during precipitation, thus playing a pivotal role in determining the final morphology and structural properties of the resulting solid.

In this study, we explored the potential of EA on generating amorphous solids of AZT initially by using pure AZT. Preliminary findings revealed that AZT consistently precipitated as an amorphous solid, as illustrated in Fig. S1 of the Supplementary Information (SI) file. Even when sufficient time was allowed for crystallization, AZT failed to form a three-dimensional crystalline structure when precipitated from solutions of EA. Subsequently, the amorphization behavior of AZT in the presence of the coformers from the library reported in Fig. 2 was investigated using a 1:1 stoichiometric ratio. This experimental data set aimed to evaluate the feasibility of creating homogeneous coamorphous systems, leveraging the properties of EA as a *bridging liquid*, i.e. mediating interactions between AZT and the coformers.

Mixtures of AZT and a specific coformer were initially milled in Retsch vibrational mill for 60 min prior to solubilization in EA. Interestingly, the mechanochemical treatment of the mixtures did not lead to the formation of coamorphous forms of AZT but rather physical mixtures of the starting materials. Indeed, PXRD analyses of the processed samples revealed little changes in the diffraction patterns (Figs. S2–S14 in the SI file). In some cases, a slight elevation of the diffractogram baseline was observed, suggesting only a partial amorphization. We therefore selected these pre-milled for subsequent solution-based experiments.

The resulting precipitates were analyzed through PXRD to assess their solid-state properties. The findings revealed that in the binary systems of AZT with A2AB, A3AB, A4AB, ASLC, MSLC, ACPL, and GLY the precipitate obtained after slow evaporation consistently presented an amorphous nature, as illustrated in Fig. 3. Indeed, the PXRD patterns

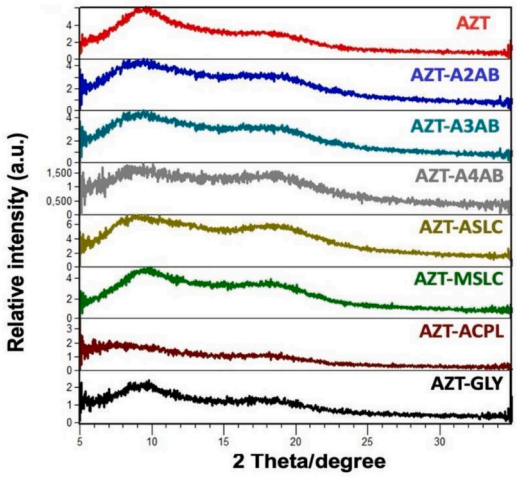

Fig. 3. Powder X-ray diffraction pattern of the products obtained from ethyl acetate evaporation after dissolving pure azithromycin and pre-milled cosystems. From top to bottom: pure azithromycin (AZT) (red), azithromycin–2-aminobenzoic acid (AZT-A2AB) (blue), azithromycin–3-aminobenzoic acid (AZT- A3AB) (teal), azithromycin–4-aminobenzoic acid (AZT-A4AB) (grey), azithromycin–salicylic acid (AZT-ASLC) (olive), azithromycin–methyl salicylate (AZT-MSLC) (green), azithromycin–caprylic acid (AZT-ACPL) (brown), and azithromycin–glycerol (AZT-GLY) (black). (For interpretation of the references to color in this figure legend, the reader is referred to the web version of this article.)

of the pure AZT and seven multicomponent systems precipitated from solutions of EA exhibited a halo typical of amorphous phase (Fig. 3).

Slow solvent evaporation also resulted an efficient preparation technique for obtaining amorphous systems; however, the extended time required for solvent removal can be a limitation, for example, during the scalability studies. We therefore optimized the process of obtaining amorphous precipitates from EA solution through rapid evaporation mode. Specifically, the pre-milled mixtures were dissolved in EA, and the solvent was rapidly removed using a rotavapor, as described in the experimental section (section 2.2.1.2). With EA boiling point at 77.1 °C [52], employing a vacuum and a thermostated bath set to 45 °C significantly accelerated solvent removal. This adjustment reduced the evaporation process from 4 days, required for slow evaporation, to only 30 min. The entire production cycle for the solid products was completed within this timeframe, marking a significant improvement in the production efficiency. The products obtained through rotavapor were confirmed to be amorphous, as evidenced by Fig. S15 in the SI file.

Subsequently, a deeper investigation into the nature of the seven new multicomponent solids was required to determine their structural and physical characteristics. Specifically, it was essential to ascertain whether these materials were physical mixtures of two separate amorphous phases or true coamorphous systems, that is a single, homogeneous amorphous phase. This distinction is critical, as a coamorphous system implies molecular-level interactions between the components, which can significantly influence the stability, dissolution rate, and overall performance of the material [23,30]. DSC analyses were therefore performed to experimentally evaluate the glass transition temperature (T_g), a defining feature of amorphous systems [53,54]. In such analyses, the detection of multiple T_g values indicates the presence of two distinct amorphous phases, suggesting that the components exist as a physical mixture with minimal or no significant interaction. In contrast, a single T_g value implies the formation of a homogeneous amorphous phase, indicative of molecular-level interactions between the components. These interactions can enhance the stability of the system and prevent phase separation [55–58]. The results of the experimental T_g values are summarized in Table 1.

Tg values were experimentally determined for pure AZT and for five out of the seven cosystems (the experimental DSC curves for each system are reported in Figs. S16–S21 in the SI file). For AZT-MSLC and AZT-GLY, the experimental determination of T_g was unsuccessful. This can be attributed to the preparation method or to the intrinsic properties of these systems. Similar cases have been reported in the literature, where milled or phase-separated amorphous products do not exhibit a clearly detectable T_g using standard DSC techniques [41,59]. It is also possible that these two samples are not true coamorphous systems, but rather two partially miscible or phase-separated amorphous domains. In such cases, the presence of two close (but unresolved) T_g values or a lack of long-term physical stability could obscure the T_g signal.

Stability is a critical factor for the practical application of amorphous systems, particularly because of the inherent tendency of these materials to revert to a crystalline state over time or under specific environmental

Table 1
Experimental glass transition values determined through differential scanning calorimetry for the coamorphous systems obtained via rotary evaporation.

Samples	Experimental glass transition (°C)
azithromycin	102.80
azithromycin–2- aminobenzoic acid	104.48
azithromycin–3-aminobenzoic acid	100.65
azithromycin–4-aminobenzoic acid	103.65
azithromycin–salicylic acid	98.77
azithromycin–methyl salicylate	/
azithromycin–caprylic acid	81.09
azithromycin–glycerol	/

'/' stands for 'not determined'.

conditions [23,41,47]. Ideally, the stability of the multicomponent system should be higher than that of the individual components due to stabilizing intermolecular interactions between the two molecules [27,58,60]. In this context, we observed that pure amorphous AZT, which was prepared via rotary evaporation and stored under ambient conditions, showed a clear tendency to recrystallize within 72 h (Fig. 4).

As previously discussed, the development of coamorphous multicomponent systems can significantly enhance physical stability by promoting the formation of stabilizing molecular interactions. These interactions reduce molecular mobility and mitigate the tendency for recrystallization, offering a clear advantage over single-component amorphous APIs [27,58,60].

Contrary to the rapid recrystallization observed for pure amorphous AZT, all seven coamorphous systems exhibited remarkable stability, maintaining their amorphous state for more than 7 days under the same ambient temperature and humidity conditions (Fig. S22 in the SI file). Given the enhanced and prolonged stability exhibited by these systems at R.T. compared to pure AZT, stability tests under more demanding conditions were subsequently performed.

Amorphous and coamorphous systems are generally considered stable below a certain temperature threshold relative to their T_g [56,61,62]. Specifically, it is commonly accepted that at temperatures approximately 50 °C below their T_g, molecular mobility is significantly reduced, minimizing the risk of physical transformations. In contrast, exceeding this temperature range can lead to a significant increase of the molecular mobility, which may trigger undesired phenomena such as recrystallization or phase separation [56,61,62]. Therefore, the coamorphous samples were stored at 40 °C, a temperature selected based on the "T_g – 50 °C rule" mentioned above. The results were highly encouraging, with five out of seven cosystems demonstrating stability after 140 days at 40 °C. Indeed, the AZT-MSLC and AZT-GLY samples, for which the T_g could not be experimentally determined, did not exhibit long-term stability and underwent recrystallization (Fig. S23-24 in the SI file). A summary of the stability tests under stressed conditions is reported in Table S1 in the SI file.

AZT-A2AB, AZT-A3AB, AZT-ASLC, and AZT-ACPL systems were identified as the most promising and selected for further advanced characterization. AZT-A4AB was excluded due to emerging deliquescence issues. Given the favorable stability profiles, the four selected systems were analyzed through PDF analyzis. This approach was employed to investigate atomic and molecular interactions across short-, medium-, and long-range distances, providing deeper insights into the structural organization and stability mechanisms of these cosystems [63–66].

As a baseline comparison, pure amorphous AZT was also analyzed 10 days post-preparation. Diffractometric analyzes revealed that the sample exhibited a partially amorphous structure with clear crystalline domains, as evidenced by distinct crystalline peaks observed in the diffraction pattern (Fig. 5). Quantitative analysis estimated the crystalline fraction to be 6.3 %, highlighting the inherent propensity of pure AZT to partially recrystallize shortly after preparation.

In contrast, all the coamorphous systems displayed diffraction patterns consistent with an amorphous nature, evidencing their structural homogeneity (see Fig. S25 in the SI file).

For example, Fig. 6 presents an overlay of the diffraction patterns for pure AZT, pure ACPL (the coformer), and their combined AZT-ACPL coamorphous. Notably, ACPL, as the only starting component in liquid form, inherently lacks crystallinity. The diffraction patterns of the coamorphous and the individual components do not overlap, demonstrating that the combined system is not a mere physical mixture of two independent amorphous substances. Instead, the observed pattern confirms that the components are thoroughly mixed at the molecular level, interacting to form a single, unified amorphous phase.

A different scenario emerges for the other starting materials, as the pure coformers are crystalline in their initial state. To further investigate the structural organization of these systems, it is essential to compare their intermolecular packing with that of pure amorphous AZT. Indeed, identifying both similarities and differences is of fundamental importance for obtaining valuable insights into the molecular interactions and stabilization mechanisms at play. Fig. 7 illustrates overlays of the diffraction patterns for each coamorphous system alongside that of amorphous AZT. The absence of residual crystalline peaks in the coamorphous systems, combined with distinct yet consistent amorphous scattering patterns, reinforces the conclusion that the coformers are thoroughly integrated into homogeneous systems. Such findings underscore the role of coamorphization in altering the molecular packing of the systems, likely driven by specific intermolecular interactions, which distinguish these systems from pure amorphous AZT.

The map presented in Fig. 7 (right) enables a detailed comparison of curve similarities. Values closer to 1 (represented by red shades in the figure, from light to dark red) represent greater overlap between curves, indicating higher similarity in molecular arrangements between the two

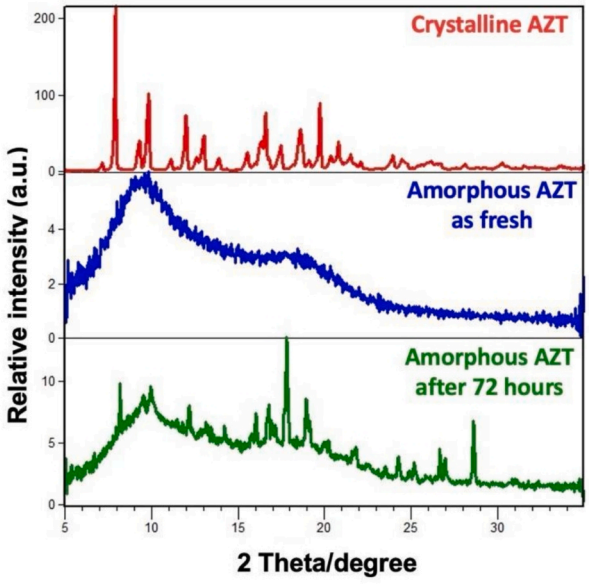

Fig. 4. Powder X-ray diffraction pattern of crystalline azithromycin (red), fresh amorphous azithromycin (blue) and amorphous azithromycin stored for 72 h (green). (For interpretation of the references to color in this figure legend, the reader is referred to the web version of this article.)

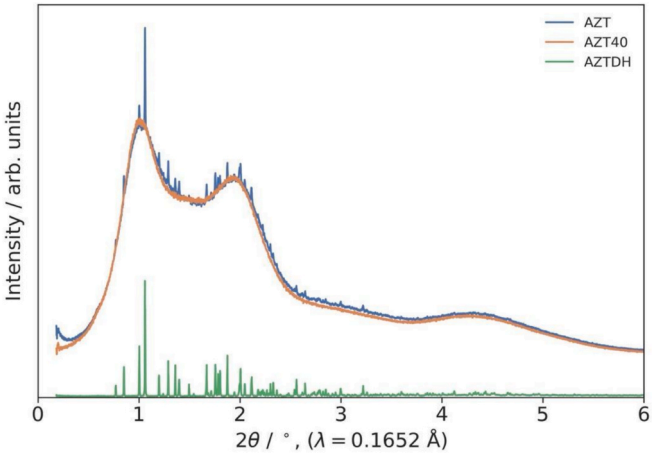

Fig. 5. Diffraction pattern of amorphous azithromycin (AZT) at 40 °C after 10 days from preparation (AZT) (blue) compared to fresh amorphous product (AZT40) (orange) and to the crystalline drug (AZTDH) (green). (For interpretation of the references to color in this figure legend, the reader is referred to the web version of this article.)

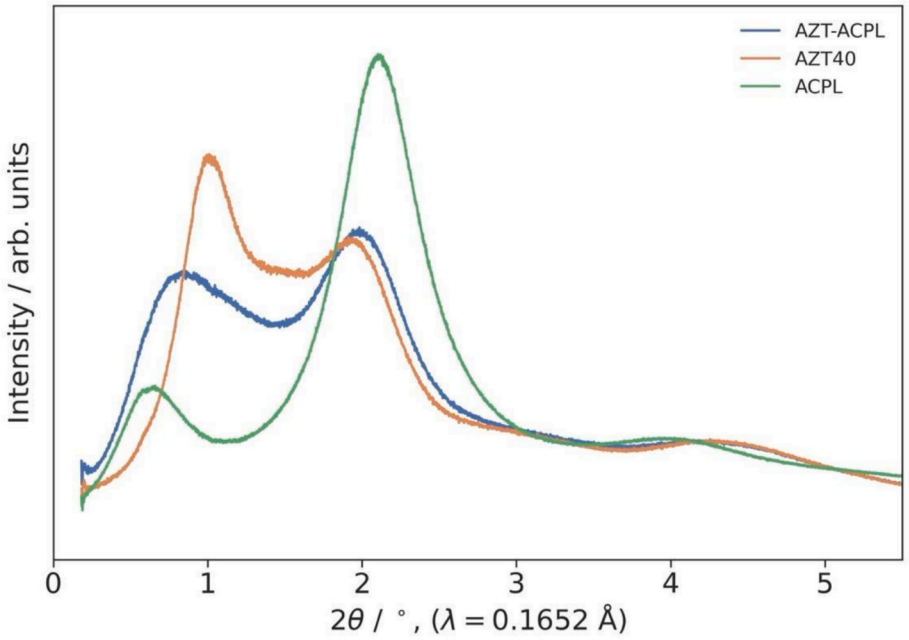

Fig. 6. PXRD pattern of pure azithromycin (AZT) (orange), pure caprylic acid (ACPL) (green) and azithromycin–caprylic acid (AZT-ACPL) coamorphous (blue). (For interpretation of the references to color in this figure legend, the reader is referred to the web version of this article.)

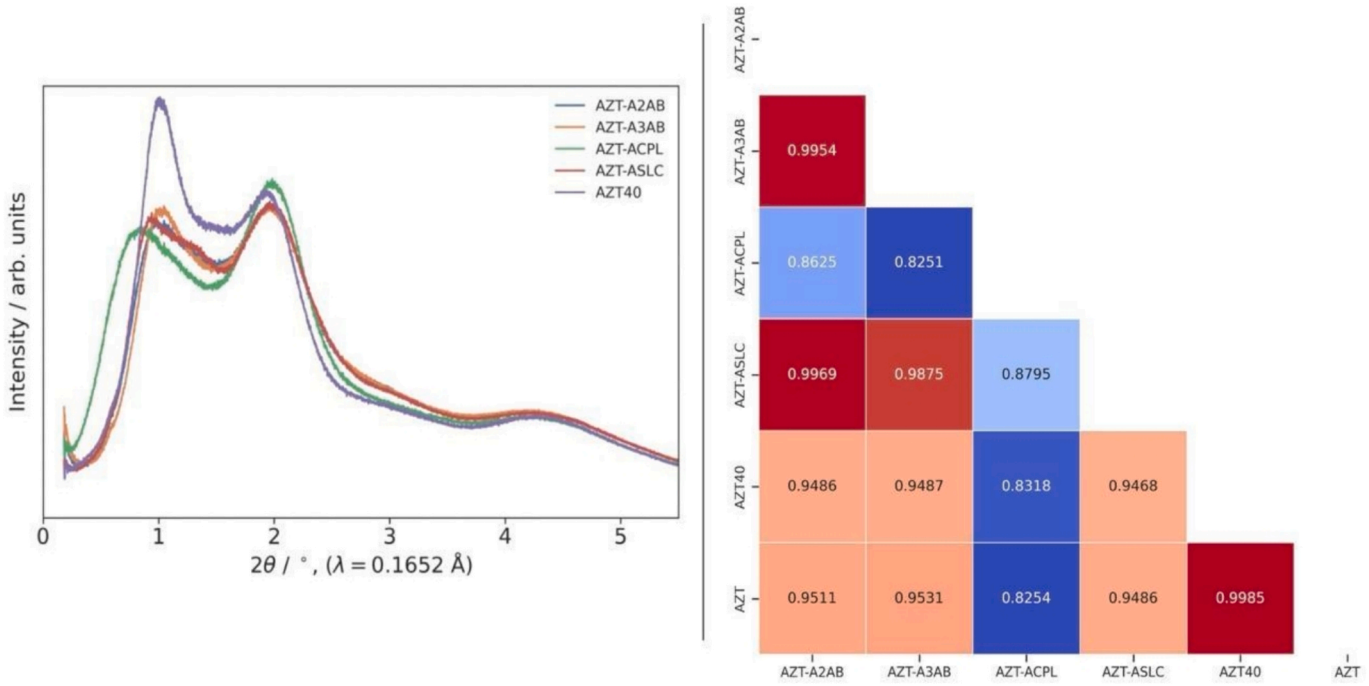

Fig. 7. On the left, an overlay of the PXRD of all multicomponent systems (azithromycin–2-aminobenzoic acid (AZT-A2AB), azithromycin–3-aminobenzoic acid (AZT- A3AB), azithromycin–caprylic acid (AZT-ACPL) and azithromycin–salicylic acid (AZT-ASLC)) and pure azithromycin (AZT). On the right, a map quantifying the similarity between the curves. The color scale reflects the degree of similarity: values close to 1 (represented by red boxes) indicate high structural resemblance between samples, while lower values (blue boxes) correspond to lower similarity. (For interpretation of the references to color in this figure legend, the reader is referred to the web version of this article.)

samples. Conversely, values progressively lower than 1 are displayed in cooler colors (from light blue to dark blue), reflecting reduced similarity and higher structural divergence. When the PXRD pattern of a specific coamorphous closely matches that of pure amorphous AZT, it suggests that the AZT molecules within the multicomponent system exhibit a similar type of structural disorder to the single-component form.

This comparative analysis highlights the critical role of the coformer in shaping the molecular organization of coamorphous systems. Notably, the systems containing A2AB, A3AB, and ACPL show distinct behaviors. The structural disorder in the coamorphous with A2AB and A3AB closely mirrors that of pure AZT, suggesting minimal disruption to the molecular arrangement of the drug in these multicomponent systems. ACPL stands out among the tested coformers due to its distinct chemical nature as a fatty acid (Fig. 2). Unlike the other coformers, its

structural characteristics introduce significant changes to the molecular packing of the coamorphous system, resulting in a unique type of structural organization.

Fig. 8 presents the PDF analysis derived using low Qmax values from both total scattering and high-resolution diffraction. This approach facilitates the examination of low-frequency oscillations, which are indicative of the absence of long-range order typical of amorphous materials. In the 4.5–9 Å range, the AZT-ACPL sample exhibits more pronounced fluctuations compared to the other multicomponent systems, suggesting a more defined intermolecular packing arrangement within this distance range. However, this trend reverses at larger distances: beyond 14 Å, the structural coherence of the AZT-ACPL sample diminishes significantly compared to the other systems. Specifically, as illustrated in Fig. 8 (right), in the 14 Å range, pure AZT and AZT-ASLC display broad oscillations that extend up to 30–35 Å, indicating the presence of intermediate-range order. By contrast, these oscillations stabilize at shorter distances for AZT-A2AB and AZT-A3AB, and even more so for AZT-ACPL, where the structural coherence is limited to smaller spatial ranges. The highlighted regions in the graph further assist in identifying the specific distance ranges where the amplitude of oscillations decreases, providing a clear visualization of the differences in structural organization among the systems. These findings highlight the unique packing characteristics of AZT-ACPL and its divergence from the other cosystems in both short- and long-range order.

The observations detailed in Fig. 8 further reinforce the differences in short- and long-range order between the three aminobenzoic acid-based samples and the AZT-ACPL system. The reduction in distances at which oscillations diminish can be attributed to a corresponding decrease in structural coherence within the AZT-ACPL system.

This reduction in coherence is consistent with the structural diversity of the coformers. A2AB and A3AB differ only by the position of a substituent, leading to relatively minor variations in molecular packing. Similarly, ASLC, which retains the core structure of the aminobenzoic acids but incorporates a distinct functional group, results in a slightly altered, yet comparable, packing arrangement. In contrast, ACPL, as a fatty acid, presents a molecular structure markedly distinct from the other coformers. This pronounced difference in structure disrupts long-range order more significantly, as reflected in the reduced coherence observed in the AZT-ACPL system.

Finally, *in vitro* dissolution tests were carried out to investigate the effect of amorphization (AZT in crystalline or amorphous form) and the use of different coformers in the multicomponent systems. As shown in Fig. 9, pure crystalline AZT showed a very slow solubilization profile, with only 12.86 ± 1.01 % of the drug dissolved in the first 2 min of analysis, and the maximum percentage of the dissolved drug (83.49 ± 1.42 %) was reached after 360 min, corresponding to the last point of the dissolution test (Fig. S26 in SI file). On the other hand, pure amorphous AZT showed a faster dissolution profile (41.73 ± 2.18 % of the active was dissolved after 2 min of analysis) with respect to the crystalline form ($p < 0.05$) and a plateau value (91.96 ± 4.22 % of drug released) was reached after 15 min. A significantly faster dissolution of AZT was observed in the coamorphous systems compared to the original crystalline AZT ($p < 0.05$). Importantly, a significant difference ($p < 0.05$) was also observed after 2 min of analysis between the coamorphous systems and pure amorphous AZT, confirming the faster release profile of AZT in the multicomponent solids. Additionally, AZT-ACPL and AZT-A3AB showed also the highest amount of drug dissolved after 2 min, leading to the dissolution of 85.97 ± 7.06 % and 84.87 ± 4.87 % of AZT, respectively, while no significant difference was observed between the two dissolution profiles of the coamorphous systems ($p > 0.05$). The faster dissolution profiles of the coamorphous systems compared to both crystalline and amorphous AZT, and an almost total dissolution of AZT-ACPL and AZT-A3AB systems in the first 2 min of analysis, highlight the effectiveness of the coamorphization technology for improving the dissolution profile of the drug.

4. Conclusions

This study successfully demonstrated the possibility of obtaining stable coamorphous systems of azithromycin, using ethyl acetate as a bridging liquid. The formation of amorphous phases was consistently achieved in seven azithromycin-based systems both via slow and rapid solvent evaporation. Differential scanning calorimetry confirmed the coamorphous nature of five systems (i.e., azithromycin–2-, 3-, and 4-aminobenzoic acids, –salicylic acid, –caprylic acid), whereas two systems (azithromycin–methyl salicylate, –glycerol) did not exhibit a detectable glass transition temperature. The absence of a glass transition temperature in these two systems likely indicated that they were not true coamorphous materials, but rather phase-separated amorphous mixtures. This hypothesis was further supported by their tendency to

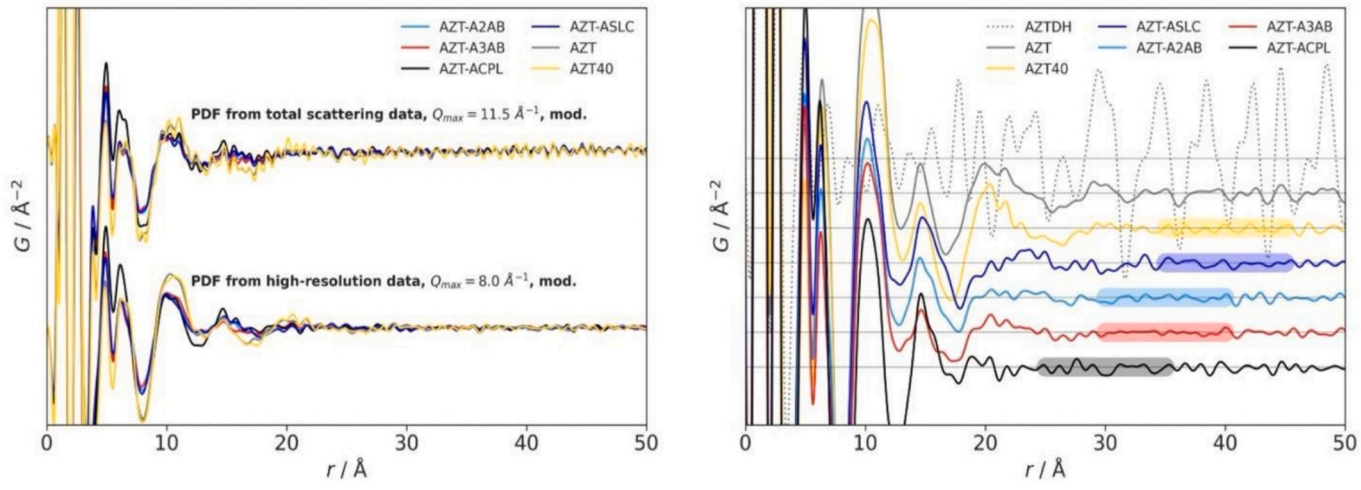

Fig. 8. On the left, a comparison of structural correlations at medium distances in the amorphous samples is shown, obtained from the PDF analysis at low Qmax values using total scattering and high-resolution diffraction. On the right, the same curves allow for the comparison of fluctuations at various distances. The highlighted sections emphasize the presence of structural coherence at specific distances. Two batches of amorphous azithromycin (at 40 °C after 10 days from preparation (AZT) (grey) compared to fresh amorphous product (AZT40) (yellow), pure crystalline commercial form (AZTDH (dotted lines)), azithromycin–2-aminobenzoic acid (AZT-A2AB) (light blue), azithromycin–3-aminobenzoic acid (AZT- A3AB) (red), azithromycin–salicylic acid (AZT-ASLC) (blue) and azithromycin–caprylic acid (AZT-ACPL) (black) are shown. (For interpretation of the references to color in this figure legend, the reader is referred to the web version of this article.)

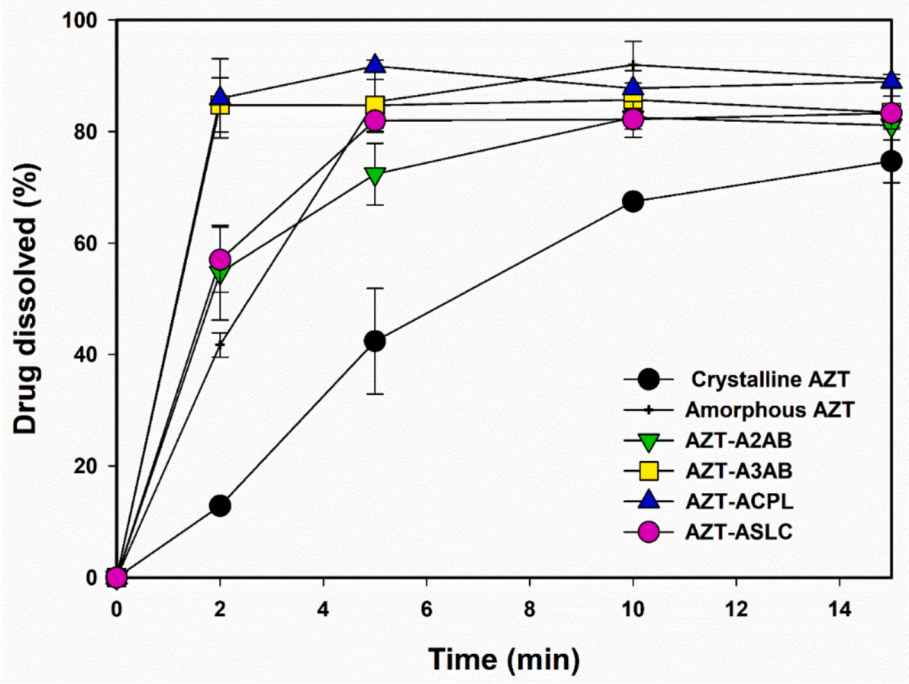

Fig. 9. Dissolution profiles obtained from crystalline azithromycin (AZT) (black circle), amorphous AZT (black dash), azithromycin–2-aminobenzoic acid (AZT-A2AB) (green triangle), azithromycin–3-aminobenzoic acid (AZT- A3AB) (yellow square), azithromycin–caprylic acid (AZT-ACPL) (blue triangle) and azithromycin–salicylic acid (AZT-ASLC) (pink circle). (For interpretation of the references to color in this figure legend, the reader is referred to the web version of this article.)

recrystallize under stress conditions, in contrast to the five confirmed coamorphous systems that remained stable for up to 140 days at 40 °C. Stability assessments further highlighted the advantages of coamorphization over the single-component amorphous form of azithromycin. While pure amorphous azithromycin, prepared via rotary evaporation, showed a clear tendency to recrystallize within 72 h under ambient conditions, all confirmed coamorphous systems exhibited significantly enhanced stability, maintaining their amorphous nature over extended periods. An advanced structural characterization of the solid-state using pair distribution function analysis provided molecular-level insights into their organization, highlighting distinct differences in molecular packing. Notably, azithromycin–caprylic acid exhibited unique structural features, forming a coamorphous solid in which the short-range order was different from that obtained during the amorphization of the pure drug. Finally, the coamorphous systems presented faster AZT dissolution properties compared to both crystalline and amorphous forms of pure AZT. The substantial improvement of the dissolution kinetics combined with the increased stability of the coamorphous systems suggests that the multicomponent systems developed in this study might be used for the development of innovative dosage forms of azithromycin.

CRediT authorship contribution statement

Ilenia D'Abbrunzo: Writing – review & editing, Writing – original draft, Validation, Methodology, Investigation, Formal analysis. **Ludovica Battaiotto:** Writing – review & editing, Writing – original draft, Validation, Methodology, Investigation, Formal analysis. **Angela Abruzzo:** Writing – review & editing, Formal analysis, Data curation. **Giulia Bondi:** Validation, Methodology, Investigation, Formal analysis. **Federica Bigucci:** Writing – review & editing. **Cinzia Pagano:** Formal analysis, Data curation. **Anna Imbriano:** Formal analysis, Data curation. **Costanza Fratini:** Formal analysis, Data curation. **Luca Casettari:** Writing – review & editing, Resources, Project administration, Formal analysis, Data curation. **Dario Voinovich:** Writing – review & editing, Supervision, Resources, Methodology, Funding acquisition. **Dritan Hasa:** Writing – review & editing, Writing – original draft, Supervision, Resources, Project administration, Funding acquisition, Conceptualization.

Declaration of competing interest

The authors declare that they have no known competing financial interests or personal relationships that could have appeared to influence the work reported in this paper.

Acknowledgements

This study is part of the "3D-printed antibiotic oral dosage forms for paediatric use [p3Diatrics]" project of Relevant National Interest (PRIN 2022) call, funded by Ministero dell'Università e della Ricerca (Project ID: 2022FRNFMT). **I.D., L.B., D.V.,** and **D.H.** would like to thank Dr Maxwell W. Terban (Momentum Transfer company) for valuable comments on PDF analysis.

Appendix A. Supplementary data

Supplementary data to this article can be found online at https://doi.org/10.1016/j.ejpb.2025.114873.

Data availability

Data will be made available on request.

References

[1] I.A. Volynkina, E.N. Bychkova, A.O. Karakchieva, A.S. Tikhomirov, G.V. Zatonsky, S.E. Solovieva, M.M. Martynov, N.E. Grammatikova, A.G. Tereshchenkov, A. Paleskava, A.L. Konevega, P.V. Sergiev, O.A. Dontsova, I.A. Osterman, A. E. Shchekotikhin, A.N. Tevyashova, Hybrid Molecules of Azithromycin with Chloramphenicol and Metronidazole: Synthesis and Study of Antibacterial Properties, Pharmaceuticals 17 (2024) 187, https://doi.org/10.3390/ph17020187.

[2] C.J. Kremer, Azithromycin—a new macrolide, Prim Care Update Ob Gyns 9 (2002) 174–175, https://doi.org/10.1016/S1068-607X(02)00112-9.
[3] C.F. MacRae, I. Sovago, S.J. Cottrell, P.T.A. Galek, P. McCabe, E. Pidcock, M. Platings, G.P. Shields, J.S. Stevens, M. Towler, P.A. Wood, Mercury 4.0: from visualization to analysis, design and prediction, J. Appl. Crystallogr. 53 (2020) 226–235, https://doi.org/10.1107/S1600576719014092.
[4] X. Cao, S. Ji, W. Kuang, A. Liao, P. Lan, J. Zhang, Solubility determination and correlation for azithromycin monohydrate and dihydrate in solvent mixtures, J. Mol. Liq. 301 (2020) 112398, https://doi.org/10.1016/j.molliq.2019.112398.
[5] M.S. Kanatani, B.J. Guglielmo, The new macrolides. Azithromycin and clarithromycin, West. J. Med. 160 (1994) 31–37. PMID: 8128699.
[6] A.A. Ali, N.A. Charoo, D.B. Abdallah, Pediatric drug development: formulation considerations, Drug Dev. Ind. Pharm. 40 (2014) 1283–1299, https://doi.org/10.3109/03639045.2013.850713.
[7] P.P. Srinivas, N. Prabhu, V. SG, N. Patel, A. Pai, V. Pai, M. Badamane Sathyanarayana, Designing of stable co-crystals of azithromycin using suitable coformers, RASAYAN J Chem 15 (2022) 2417–2428. 10.31788/RJC.2022.1546985.
[8] N. Ul Islam, E. Khan, M. Naveed Umar, A. Shah, M. Zahoor, R. Ullah, A. Bari, Enhancing Dissolution Rate and Antibacterial Efficiency of Azithromycin through Drug-Drug Cocrystals with Paracetamol, Antibiotics 10 (2021) 939, https://doi.org/10.3390/antibiotics10080939.
[9] K.P. Upadhye, C.S. Dhakate, G.R. Dixit, S.S. Bakhle, Development and Evaluation of Taste Masked Azithromycin by Crystal Engineering, Int J Drug Deliv Technol 11 (2021) 920–925. 10.25258/ijddt.11.3.46.
[10] CN100427499C - Soluble salt of azithromycin and its preparation process - Google Patents, https://patents.google.com/patent/CN100427499C/en (accessed March 25, 2025).
[11] WO2004106355A1 - Addition salts of azithromycin and citric acid and process for preparing them - Google Patents, https://patents.google.com/patent/WO2004106355A1/en (accessed March 25, 2025).
[12] E. Adeli, Preparation and evaluation of azithromycin binary solid dispersions using various polyethylene glycols for the improvement of the drug solubility and dissolution rate, Brazilian, J. Pharm. Sci. 52 (2016) 1–13, https://doi.org/10.1590/S1984-82502016000100002.
[13] S.C. Arora, P.K. Sharma, R. Irchhaiya, A. Khatkar, N. Singh, J. Gagoria, Development, characterization and solubility study of solid dispersions of azithromycin dihydrate by solvent evaporation method, J. Adv. Pharm. Technol. Res. 1 (2010) 221–228.
[14] S.S. Zinjad, D.A. Udmale, A.D. Suryawanshi, S.L. Jadhav, D.D. Gaikwad, Solubility Enhancment of Azithromycin by Solid Dispersion Method by using Polymer PVP K 90, J Drug Deliv Therap 9 121–124 (2019) 10.22270/jddt.v9i3.2617.
[15] J. Li, C. Li, H. Zhang, X. Gao, T. Wang, Z. Wang, A. Zheng, Preparation of Azithromycin Amorphous Solid Dispersion by Hot-Melt Extrusion: an Advantageous Technology with taste Masking and Solubilization Effects, Polymers (basel) 14 (2022) 495, https://doi.org/10.3390/polym14030495.
[16] M. Raval, H. Bagada, Formulation and Evaluation of Cyclodextrin-based Thermosensitive In Situ Gel of Azithromycin for Periodontal delivery, J. Pharm. Innov. 16 (2021) 67–84, https://doi.org/10.1007/s12247-019-09422-3.
[17] D. Boczar, K. Michalska, Cyclodextrin Inclusion Complexes with Antibiotics and Antibacterial Agents as Drug-delivery Systems—A Pharmaceutical Perspective, Pharmaceutics 14 (2022) 1389, https://doi.org/10.3390/pharmaceutics14071389.
[18] S. Bhattacharyya, P. Reddy, Effect of Surfactant on Azithromycin Dihydrate Loaded Stearic Acid Solid Lipid Nanoparticles., Turk, J. Pharm. Sci. 16 (2019) 425–431, https://doi.org/10.4274/tjps.galenos.2018.82160.
[19] J.Y. Wu, Q. Xia, Preparation and Characterization of Azithromycin-Loaded Nanostructured Lipid Carriers, Adv. Mat. Res. 236–238 (2011) 2917–2920, https://doi.org/10.4028/www.scientific.net/AMR.236-238.2917.
[20] V.S. Solleti, M. Alhariri, M. Halwani, A. Omri, Antimicrobial properties of liposomal azithromycin for Pseudomonas infections in cystic fibrosis patients, J. Antimicrob. Chemother. 70 (2015) 784–796, https://doi.org/10.1093/jac/dku452.
[21] M.A. Bazán Henostroza, G. Diniz Tavares, M. Nishitani Yukuyama, A. De Souza, E. José Barbosa, V. Carlos Avino, E. dos Santos Neto, F. Rebello Lourenço, R. Löbenberg, N. Araci Bou-Chacra, Antibiotic-loaded lipid-based nanocarrier: a promising strategy to overcome bacterial infection, Int J Pharm 621 (2022) 121782, https://doi.org/10.1016/j.ijpharm.2022.121782.
[22] C.R. Groom, I.J. Bruno, M.P. Lightfoot, S.C. Ward, The Cambridge Structural Database, Acta Crystallogr B Struct Sci Cryst Eng Mater 72 (2016) 171–179, https://doi.org/10.1107/S2052520616003954.
[23] N. Chieng, J. Aaltonen, D. Saville, T. Rades, Physical characterization and stability of amorphous indomethacin and ranitidine hydrochloride binary systems prepared by mechanical activation, Eur. J. Pharm. Biopharm. 71 (2009) 47–54, https://doi.org/10.1016/j.ejpb.2008.06.022.
[24] K. Holzapfel, T. Rades, C.S. Leopold, Co-amorphous systems consisting of indomethacin and the chiral co-former tryptophan: Solid-state properties and molecular mobilities, Int. J. Pharm. 636 (2023) 122840, https://doi.org/10.1016/J.IJPHARM.2023.122840.
[25] G. Kasten, K. Löbmann, H. Grohganz, T. Rades, Co-former selection for co-amorphous drug-amino acid formulations, Int. J. Pharm. 557 (2018) 366–373, https://doi.org/10.1016/j.ijpharm.2018.12.036.
[26] S.J. Dengale, H. Grohganz, T. Rades, K. Löbmann, Recent advances in co-amorphous drug formulations, Adv. Drug Deliv. Rev. 100 (2016) 116–125, https://doi.org/10.1016/j.addr.2015.12.009.
[27] W. Wu, Y. Wang, K. Löbmann, H. Grohganz, T. Rades, Transformations between Co-Amorphous and Co-Crystal Systems and their Influence on the Formation and Physical Stability of Co-Amorphous Systems, Mol. Pharm. 16 (2019) 1294–1304, https://doi.org/10.1021/acs.molpharmaceut.8b01229.
[28] R. Laitinen, K. Löbmann, C.J. Strachan, H. Grohganz, T. Rades, Emerging trends in the stabilization of amorphous drugs, Int. J. Pharm. 453 (2013) 65–79, https://doi.org/10.1016/j.ijpharm.2012.04.066.
[29] J. Liu, H. Grohganz, K. Löbmann, T. Rades, N.-J. Hempel, Co-Amorphous Drug Formulations in Numbers: recent advances in Co-Amorphous Drug Formulations with Focus on Co-Formability, Molar Ratio, Preparation Methods, Physical Stability, in Vitro and in Vivo Performance, and New Formulation Strategies, Pharmaceutics 13 (2021) 389, https://doi.org/10.3390/pharmaceutics13030389.
[30] N.A. Vasilev, A.P. Voronin, A.O. Surov, G.L. Perlovich, Influence of Co-amorphization on the Physical Stability and Dissolution Performance of an Anthelmintic Drug Flubendazole, Mol. Pharm. 20 (2023) 1657–1669, https://doi.org/10.1021/acs.molpharmaceut.2c00873.
[31] I. D'Abbrunzo, E. Venier, F. Selmin, I. Škorić, E. Bernardo, G. Procida, B. Perissutti, Stability of Ternary Drug–Drug–Drug Coamorphous Systems Obtained through Mechanochemistry, Pharmaceutics 17 (2025) 92, https://doi.org/10.3390/pharmaceutics17010092.
[32] B. Li, Y. Wang, Y. Feng, D. Yuan, R. Xu, C. Jiang, X. Xiao, S. Lu, Design and molecular insights of drug-active metabolite based co-amorphous formulation: a case study of toltrazuril-ponazuril co-amorphous, Int. J. Pharm. 615 (2022) 121475, https://doi.org/10.1016/j.ijpharm.2022.121475.
[33] K. Ueda, D.E. Moseson, L.S. Taylor, Amorphous solubility advantage: Theoretical considerations, experimental methods, and contemporary relevance, J. Pharm. Sci. 114 (2025) 18–39, https://doi.org/10.1016/j.xphs.2024.08.029.
[34] P. Karmwar, K. Graeser, K.C. Gordon, C.J. Strachan, T. Rades, Effect of different preparation methods on the dissolution behaviour of amorphous indomethacin, Eur. J. Pharm. Biopharm. 80 (2012) 459–464, https://doi.org/10.1016/j.ejpb.2011.10.006.
[35] A. Newman, G. Knipp, G. Zografi, Assessing the performance of amorphous solid dispersions, J. Pharm. Sci. 101 (2012) 1355–1377, https://doi.org/10.1002/jps.23031.
[36] R. Laitinen, P.A. Priemel, S. Surwase, K. Graeser, C.J. Strachan, H. Grohganz, T. Rades, Theoretical Considerations in Developing Amorphous Solid Dispersions, Advances in Delivery Science and Technology in: Springer (New York) (2014) 35–90. 10.1007/978-1-4939-1598-9_2.
[37] E. Kaminska, K. Adrjanowicz, D. Zakowiecki, B. Milanowski, M. Tarnacka, L. Hawelek, M. Dulski, J. Pilch, W. Smolka, I. Kaczmarczyk-Sedlak, K. Kaminski, Enhancement of the Physical Stability of Amorphous Indomethacin by Mixing it with Octaacetylmaltose, Inter and Intra Molecular Studies, Pharm Res 31 (2014) 2887–2903, https://doi.org/10.1007/s11095-014-1385-4.
[38] W. Heng, Y. Song, M. Luo, E. Hu, Y. Wei, Y. Gao, Z. Pang, J. Zhang, S. Qian, Mechanistic insights into the crystallization of coamorphous drug systems, JCR 354 (2023) 489–502, https://doi.org/10.1016/j.jconrel.2023.01.019.
[39] J. Li, N.K. Duggirala, N.S.K. Kumar, Y. Su, R. Suryanarayanan, Design of Ternary Amorphous Solid Dispersions for Enhanced Dissolution of Drug Combinations, Mol. Pharm. 19 (2022) 2950–2961, https://doi.org/10.1021/acs.molpharmaceut.2c00307.
[40] N.J. Babu, A. Nangia, Solubility Advantage of Amorphous Drugs and Pharmaceutical Cocrystals, Cryst. Growth Des. 11 (2011) 2662–2679, https://doi.org/10.1021/cg200492w.
[41] Q. Shi, S.M. Moinuddin, T. Cai, Advances in coamorphous drug delivery systems, Acta Pharm. Sin. B 9 (2019) 19–35, https://doi.org/10.1016/j.apsb.2018.08.002.
[42] A. Gabelmann, C.-M. Lehr, H. Grohganz, Preparation of Co-Amorphous Levofloxacin Systems for Pulmonary Application, Pharmaceutics 15 (2023) 1574, https://doi.org/10.3390/pharmaceutics15061574.
[43] B. Li, Y. Hu, Y. Guo, R. Xu, X. Fang, X. Xiao, C. Jiang, S. Lu, Coamorphous System of Florfenicol-Oxymatrine for improving the Solubility and Dissolution Rate of Florfenicol: Preparation, Characterization and Molecular Dynamics simulation, J. Pharm. Sci. 110 (2021) 2544–2554, https://doi.org/10.1016/j.xphs.2021.02.005.
[44] L.H.S. Queiroz, R.S. Barros, F.F. de Sousa, M.R. Lage, M.C. Sarraguça, P.R. S. Ribeiro, Preparation and Characterization of a Rifampicin Coamorphous Material with Tromethamine Coformer: an Experimental–Theoretical Study, Mol. Pharm. 21 (2024) 1272–1284, https://doi.org/10.1021/acs.molpharmaceut.3c00947.
[45] Z. Wang, X. Chen, D. Li, E. Bai, H. Zhang, Y. Duan, Y. Huang, Platensimycin-berberine chloride co-amorphous drug system: Sustained release and prolonged half-life, Eur. J. Pharm. Biopharm. 179 (2022) 126–136, https://doi.org/10.1016/j.ejpb.2022.09.002.
[46] T. Friščić, S.L. Childs, S.A.A. Rizvi, W. Jones, The role of solvent in mechanochemical and sonochemical cocrystal formation: a solubility-based approach for predicting cocrystallisation outcome, CrstEngComm 11 (2009) 418–426, https://doi.org/10.1039/B815174A.
[47] T. Xie, L.S. Taylor, Effect of Temperature and Moisture on the Physical Stability of Binary and Ternary Amorphous Solid Dispersions of Celecoxib, J. Pharm. Sci. 106 (2017) 100–110, https://doi.org/10.1016/j.xphs.2016.06.017.
[48] European Synchrotron Radiation Facility (ESRF), https://www.esrf.fr/ (accessed November 23, 2024).
[49] Fast Azimuthal Integration using Python — pyFAI 2024.9.0 documentation, https://pyfai.readthedocs.io/en/stable/ (accessed November 23, 2024).
[50] A. Abruzzo, C. Parolin, M. Rossi, B. Vitali, C. Cappadone, F. Bigucci, Development and Characterization of Azithromycin-Loaded Microemulsions: a Promising Tool

for the Treatment of Bacterial Skin Infections, Antibiotics 11 (2022) 1040, https://doi.org/10.3390/antibiotics11081040.
[51] K. Chen, B. Hou, H. Wu, X. Huang, F. Li, Y. Xiao, J. Li, Y. Bao, H. Hao, Hollow and Solid Spherical Azithromycin Particles Prepared by Different Spherical Crystallization Technologies for Direct Tableting, Processes 7 (2019) 276, https://doi.org/10.3390/pr7050276.
[52] Ethyl Acetate | CH3COOC2H5 | CID 8857 - PubChem, https://pubchem.ncbi.nlm.nih.gov/compound/8857 (accessed November 23, 2024).
[53] Z.H. Stachurski, On Structure and Properties of Amorphous Materials, Materials 4 (2011) 1564–1598, https://doi.org/10.3390/ma4091564.
[54] C. Červinka, M. Fulem, Structure and Glass transition Temperature of Amorphous Dispersions of Model Pharmaceuticals with Nucleobases from Molecular Dynamics, Pharmaceutics 13 (2021) 1253, https://doi.org/10.3390/pharmaceutics13081253.
[55] W.L. Chiou, S. Riegelman, Pharmaceutical applications of Solid Dispersion Systems, J. Pharm. Sci. 60 (1971) 1281–1302, https://doi.org/10.1002/jps.2600600902.
[56] B.C. Hancock, S.L. Shamblin, G. Zografi, Molecular Mobility of Amorphous Pharmaceutical Solids Below their Glass transition Temperatures, Pharm. Res. 12 (1995) 799–806, https://doi.org/10.1023/A:1016292416526.
[57] Q. Lu, G. Zografi, Phase behavior of binary and ternary amorphous mixtures containing indomethacin, citric acid and PVP, Pharm. Res. 15 (1998) 1202–1206, https://doi.org/10.1023/A:1011983606606.
[58] J. Buitink, I.J. van den Dries, F.A. Hoekstra, M. Alberda, M.A. Hemminga, High critical Temperature above Tg May Contribute to the Stability of Biological Systems, Biophys. J . 79 (2000) 1119–1128, https://doi.org/10.1016/S0006-3495(00)76365-X.
[59] T. Feng, S. Bates, M.T. Carvajal, Toward understanding the evolution of griseofulvin crystal structure to a mesophase after cryogenic milling, Int. J. Pharm. 367 (2009) 16–19, https://doi.org/10.1016/j.ijpharm.2008.10.011.
[60] A. Alhalaweh, A. Alzghoul, D. Mahlin, C.A.S. Bergström, Physical stability of drugs after storage above and below the glass transition temperature: Relationship to glass-forming ability, Int. J. Pharm. 495 (2015) 312–317, https://doi.org/10.1016/j.ijpharm.2015.08.101.
[61] G. Van den Mooter, The use of amorphous solid dispersions: a formulation strategy to overcome poor solubility and dissolution rate, Drug Discov. Today Technol. 9 (2012) e79–e85, https://doi.org/10.1016/j.ddtec.2011.10.002.
[62] M. Yoshioka, B.C. Hancock, G. Zografi, Crystallization of Indomethacin from the Amorphous State below and above its Glass transition Temperature, J. Pharm. Sci. 83 (1994) 1700–1705, https://doi.org/10.1002/jps.2600831211.
[63] S.J.L. Billinge, Total scattering and atomic pair distribution function analysis: overview and applications. https://www.bnl.gov/pdfschool2018/files/2018-talks/billinge.pdf (accessed November 23, 2024).
[64] M.W. Terban, S.J.L. Billinge, Structural Analysis of Molecular Materials using the Pair distribution Function, Chem. Rev. 122 (2022) 1208–1272, https://doi.org/10.1021/acs.chemrev.1c00237.
[65] S.J.L. Billinge, The rise of the X-ray atomic pair distribution function method: a series of fortunate events, Philos. Transact. A Math. Phys. Eng. Sci. 377 (2019) 20180413, https://doi.org/10.1098/rsta.2018.0413.
[66] Th. Proffen, S.J.L. Billinge, T. Egami, D. Louca, Structural analysis of complex materials using the atomic pair distribution function — a practical guide, Z Kristallogr Cryst Mater 218 (2003) 132–143, https://doi.org/10.1524/zkri.218.2.132.20664.